

Effect of dopants on thermal stability and self-diffusion in iron nitride thin films

Akhil Tayal, Mukul Gupta* and Ajay Gupta

UGC-DAE Consortium for Scientific Research, University Campus, Khandwa Road, Indore 452 001, India

M. Horisberger¹ and Jochen Stahn²

¹LDM, ²LNS, Paul Scherrer Institut, CH-5232 Villigen PSI, Switzerland

Kai Schlage and H.-C. Wille

Deutsches Elektronen-Synchrotron DESY, Notkestrasse 85, D-22607 Hamburg, Germany

(Dated: June 16, 2014)

We studied the effect of dopants (Al, Ti, Zr) on the thermal stability of iron nitride thin films prepared using a dc magnetron sputtering technique. Structure and magnetic characterization of deposited samples reveal that the thermal stability together with soft magnetic properties of iron nitride thin films get significantly improved with doping. To understand the observed results, detailed Fe and N self-diffusion measurements were performed. It was observed that N self-diffusion gets suppressed with Al doping whereas Ti or Zr doping results in somewhat faster N diffusion. On the other hand Fe self-diffusion seems to get suppressed with any dopant of which heat of nitride formation is significantly smaller than that of iron nitride. Importantly, it was observed that N self-diffusion plays only a trivial role, as compared to Fe self-diffusion, in affecting the thermal stability of iron nitride thin films. Based on the obtained results effect of dopants on self-diffusion process is discussed.

I. INTRODUCTION

Iron nitride (Fe-N) compounds exist in a variety of phases having distinct crystal structure and magnetic properties.¹ These compounds have gained a special attention for their numerous technological applications such as in tribological coatings, magnetic memory devices, high frequency read write heads etc.^{2–10} Different Fe-N phases can be formed by varying the nitrogen concentration in Fe.¹¹ When N concentration is less than 25at.%, Fe-N compounds are ferromagnetic and their Curie temperature is above room temperature. Strikingly, within the composition range $0 < N \leq 11$ at.%, Fe-N compounds possess interesting magnetic properties and major phases formed are α -Fe, Fe_8N and $\alpha''\text{-Fe}_{16}\text{N}_2$.^{12,13} In this composition range, N atoms get mainly occupied at random-interstitial sites within the *bcc* Fe lattice. This creates some distortion in the lattice and results in nanocrystallization, which improves soft-magnetic properties and favors magnetic anisotropy.^{14–17} Around the saturation concentration i.e. ~ 11 at.% instead of random occupancy, N atoms get perfectly ordered to form $\alpha''\text{-Fe}_{16}\text{N}_2$ phase having *bct* structure.¹⁸ At around 20at.% of N $\gamma'\text{-Fe}_4\text{N}$ phase is formed having *fcc* structure. These Fe-N phases have tremendous applications due to their ingenious magnetic properties.^{2–4,9,10,19,20} However, weak Fe and N bonding results in poor thermal stability of Fe-N compounds.^{21–25} It causes a severe limitation for Fe-N compounds to succeed as a potential candidate for device applications.

Recently, it was shown that doping of a third element, say X (e.g. Al, Ti, Zr, Ta, etc.) results in superior thermal stability of Fe-N thin films.^{15,25–44} These dopants either get dissolved substitutionally into the Fe lattice or form a solid solution with Fe, which also creates some

lattice distortion. Importantly, the qualifying thermodynamical variables that are required to enhance the thermal stability are high affinity (f) and low heat of formation (ΔH) of X-N as compared to Fe-N. It has been established in the literature that high X-N bonding may suppress N diffusion to enhance the thermal stability of resultant Fe-X-N thin films.⁴⁵ Although, no direct diffusion measurements are available to support such arguments, besides, the role of Fe self-diffusion is also not yet clearly established. Apart from it, on the basis of this assumption, it is expected that X with the highest affinity for N and the smallest ΔH should be an ideal choice. However, numerous studies that were made using various dopants gives a diverse picture on their role in affecting the structure, magnetic properties and thermal stability that makes the choice of dopants rather arbitrary.^{15,25,27,33,35,37} In some studies, it was observed that doping of Al or Ta improves the soft magnetic properties. Even so, thermal stability is found to get better with Al addition as compared to Ta.^{37,46} It was claimed that large atomic size of Ta results in a lower diffusion barrier for the interstitial nitrogen. On the contrary, Chechenin *et al.* found that nitrogen desorption get reduced by addition of Zr, although the atomic size of Zr and Ta is almost equal.²⁵ Similarly, addition of Ti have found to affect various magnetic properties and significantly enhance the thermal stability of Fe-N thin films, even through its atomic size is larger than Fe.^{15,47}

Above scenario suggests that beside the thermodynamic parameters ΔH and f , atomic size of X may play a decisive role in improving the thermal stability of Fe-N thin films. Table I compares these parameters for the dopants mostly used in Fe-X-N thin films.^{45,48–50} From table I, it can be seen that Zr and Al are on extreme ends with reference to their affinity and atomic size. Although

their heat of nitride formation is somewhat similar, still significantly lower as compared to magnetic Fe-N. Therefore, it will be interesting to compare the effect of Al and Zr doping on thermal stability and atomic diffusion. To the best of our knowledge this is a first study correlating the effect of nitrogen and iron self-diffusion and thermal stability in Fe-N thin films. To obtain a conclusive picture, N self-diffusion measurements were also performed on Ti doped sample, as Ti doping has also been extensively used in literature.^{44,47,51}

TABLE I. Atomic radius (r), heat of formation (ΔH) and affinity (f) of X-N with respect to Fe-N.

Element	$r(\text{pm})$	$\Delta H (\text{kJ mol}^{-1})$	f
Zr	206	-360	-0.63
Ti	176	-338	-0.53
Ta	200	-237	-0.032
Al	118	-321	-0.028
Fe	146	-10	-

II. EXPERIMENTAL

Fe-X-N thin film samples with $X = \text{Al, Ti or Zr}$, were deposited using a dc-magnetron sputtering technique simultaneously on Si(100) and float glass substrates at room temperature. Pure Fe, [Fe+Al], [Fe+Ti] and [Fe+Zr] composite targets were sputtered using a mixture of N_2 (1.5 sccm) and Ar(8.5 sccm) gases. To get the desired composition of Al, Ti and Zr, relative coverage of Al, Ti or Zr on Fe target was varied taking into account their relative sputter yields. Composition of deposited samples was measured using energy dispersive X-ray analysis and secondary neutral mass spectroscopy and comes out to be $5.6(\pm 1.2)\text{at.}\%$ for Al, $4.1(\pm 1.4)\text{at.}\%$ for Ti, and $3.2(\pm 1.3)\text{at.}\%$ for Zr. The composition of nitrogen was measured with secondary ion mass spectroscopy using a reference sample of known composition and comes out to be $\sim 11\text{at.}\%(\pm 1)$ in all the samples. This was also confirmed using conversion electron Mössbauer spectroscopy in the un-doped sample. A base pressure of about 1×10^{-7} mbar was achieved prior to the deposition. During the deposition, partial pressure in the chamber was about 4×10^{-3} mbar. More details about the deposition system are given elsewhere.^{14,24}

Multilayer samples with nominal structure: substrate|[$^{nat}\text{Fe-X-N}(6\text{ nm})|^{57}\text{Fe-X-N}(6\text{ nm})$] $\times 10$ and substrate|[Fe-X- $^{nat}\text{N}(9\text{ nm})|$ Fe-X- $^{15}\text{N}(9\text{ nm})$] $\times 25$ were prepared for Fe and N self-diffusion measurements using neutron reflectivity, with $X = 0, \text{Al, Ti, and Zr}$. Here ‘ nat ’ indicates isotopes of Fe and N obtained in natural abundance. Isotope enrichment of ^{57}Fe layers exceeds to about 95%, and that of ^{15}N is about 98%. For N diffusion measurements with secondary ion mass spectroscopy a special trilayer structure: substrate|[Fe-X- $^{nat}\text{N}(110\text{ nm})|$ Fe-X- $^{15}\text{N}(2\text{ nm})|$ Fe-X- $^{nat}\text{N}(110\text{ nm})$], with $X = 0, \text{Al, Zr}$ was deposited. Such structure is expected to give a peak when looking at ^{15}N depth profile.

For Fe diffusion measurements with nuclear resonance reflectivity, substrate|[$^{nat}\text{Fe-N}(2.2\text{ nm})|^{57}\text{Fe-N}(2.2\text{ nm})$] $\times 10$ and substrate|[$^{nat}\text{Fe-Al-N}(2\text{ nm})|^{57}\text{Fe-Al-N}(2\text{ nm})$] $\times 10$ samples were deposited. All samples were deposited using identical deposition condition. Samples with $X = 0, \text{Al, Zr and Ti}$ are named as Fe-N, Fe-Al-N, Fe-Zr-N, Fe-Ti-N, respectively through out this work.

Structural characterization was done using X-ray diffraction (XRD) on a Bruker D8 Advance X-ray diffractometer with Cu $K\alpha$ X-ray source in $\theta - 2\theta$ geometry. Magnetic properties were studied using Quantum Design superconducting quantum interference device-vibrating sample magnetometer (S-VSM) and conversion electron Mössbauer spectroscopy (CEMS). Self-diffusion measurements of Fe was performed using polarized neutron reflectivity (PNR) and nuclear resonance reflectivity (NRR). For N self-diffusion measurements PNR and secondary ion mass spectrometry (SIMS) techniques were used. The PNR measurements were carried out on AMOR reflectometer at SINQ, PSI Switzerland. A magnetic field of about 400 kA/m was applied to saturate the samples magnetically. For diffusion measurements only spin up reflectivity were used. The NRR measurements were performed using 14.4 keV radiation at P01 beamline, PETRA III, DESY, Germany. SIMS measurements were performed on a Hiden Analytical SIMS Workstation. A base pressure of 8×10^{-10} mbar was achieved in the SIMS chamber. A beam of O_2^+ primary ions (energy 5 keV and current 400 nA) was used to sputter samples. During measurements pressure in the chamber was about 8×10^{-8} mbar. To investigate the thermal stability and to measure self-diffusivity *ex-situ* annealing of samples was performed in a separate vacuum chamber.

III. RESULTS

A. X-ray diffraction

Fig. 1 (a)-(c) shows the XRD patterns of Fe-N, Fe-Al-N and Fe-Zr-N samples in the as-deposited state and after annealing at various temperatures. XRD patterns taken at selective temperatures are shown in the figure. From fig. 1(a) it can be seen that in the as-deposited state distinct broad peaks corresponding to *bcc* $\alpha\text{-Fe(N)}$ and $\alpha''\text{-Fe}_{16}\text{N}_2$ phase are appearing.⁵² It is known that in these phases nitrogen atoms are occupied within the interstitial sites of Fe lattice in random and ordered fashion, respectively.¹³ With annealing up to 450 K peak intensity increases and the width reduces indicating an enhancement in nitrogen ordering. Above this temperature α'' phase almost disappears. With further annealing, intensity of the peak corresponding to $\gamma'\text{-Fe}_4\text{N}$ rises implying the growth of γ' phase. On contrary to this, the behavior of Fe-Al-N and Fe-Zr-N samples is different. From fig. 1(b-c) it can be seen that in the as-deposited state, only peaks corresponding to $\alpha\text{-Fe(N)}$ phase are observed. Annealing of the samples up to 500 K shows no change in

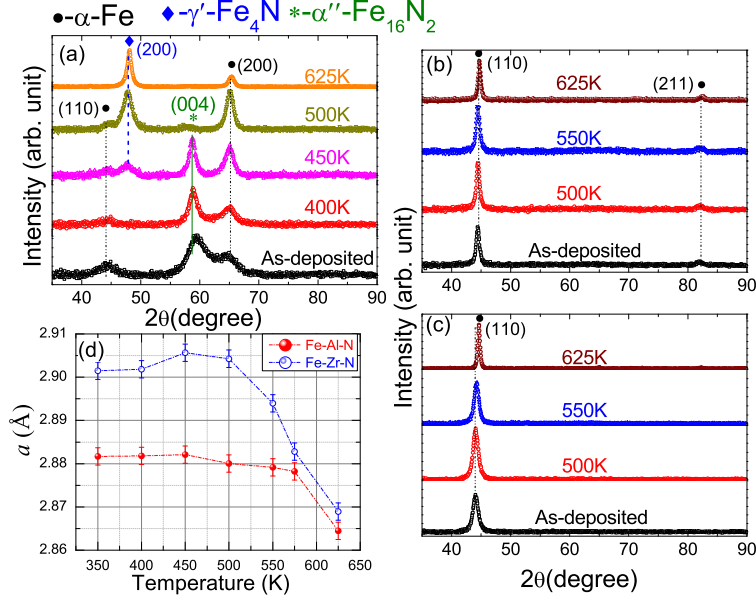


FIG. 1. (color online) XRD patterns of Fe-N(a), Fe-Al-N(b) and Fe-Zr-N(c) samples in the as-deposited state and after annealing at various temperatures. For better comparison scales are vertically translated. Variation of lattice constant with annealing temperature for Fe-Al-N and Fe-Zr-N samples(d).

the XRD pattern. Moreover, no extra peaks corresponding to any other phases can be seen even after 625 K. This indicates that thermal stability of the films gets significantly improved with doping. From (110) reflection, average crystallite size in the samples was calculated using Scherrer formula⁵³ and found to be 15 nm and 9 nm for Fe-Al-N and Fe-Zr-N samples, respectively. Moreover, lattice constant (a) of doped samples in the as-deposited state is compared with un-doped samples. It was observed that with Al doping average volume of Fe unit cell get reduced to about 0.5%, whereas, in case of Zr it get increased by about 2%. This results can be attributed to the varied atomic size of Al and Zr with respect to Fe. For doped samples it can be seen that the peak position corresponding to the (110) reflection shifts to higher 2θ above 500 K. Fig. 1(d) shows variation of the lattice constant with annealing temperature for Fe-Al-N and Fe-Zr-N samples. Up to 575 K ' a ' remains almost constant with Al doping, while it shows a marginal increase above 400 K and a step decrease above 575 K. Whereas with Zr doping step decrease in ' a ' starts already at 500 K. It signifies that Al doping results in relatively superior structural stability.

B. Magnetic measurements

From the XRD results discussed in section III A, it was found that the as-deposited state of Fe-N thin film comprises of α -Fe(N) and α'' -Fe₁₆N₂ phases and in Fe-Al-N and Fe-Zr-N samples, only α -Fe(N) phase is observed. To investigate the implication of different structure on the magnetic properties, we did M-H (magnetization-

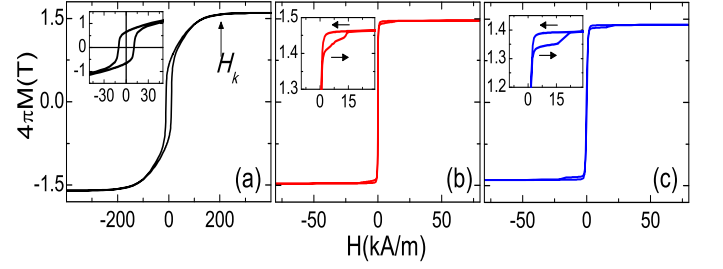


FIG. 2. (color online) M-H loops of as-deposited Fe-N(a), Fe-Al-N(b) and Fe-Zr-N(c) thin films. Inset of figure shows a blown up region near the coercive field. Arrows in (b,c) show direction of applied magnetic field during M-H measurements.

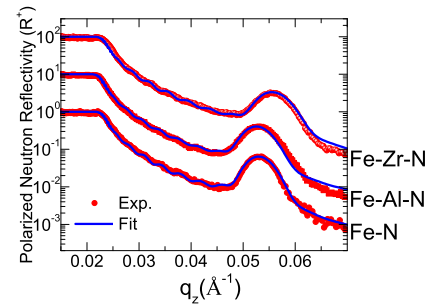


FIG. 3. (color online) Spin-up reflectivity patterns of as-deposited Sub.[Fe-N(6.53 nm)]⁵⁷Fe-N(6.53 nm)₁₀, Sub.[Fe-Al-N(6.55 nm)]⁵⁷Fe-Al-N(6.55 nm)₁₀, and Sub.[Fe-Zr-N(6.15 nm)]⁵⁷Fe-Zr-N(6.15 nm)₁₀ thin films. Patterns are vertically translated for clarity.

applied magnetic field) measurements. Fig. 2(a-c) shows M-H loops of the as-deposited samples. The inset in figures shows a blown up region near the coercive field. A typical ‘*transcritical shape*’ of the M-H loop (fig. 2(a)) for un-doped sample suggests that the film exhibits perpendicular magnetic anisotropy (PMA). Recently, Ji *et al.* have reported similar type M-H loops for epitaxial $\alpha''\text{-Fe}_{16}\text{N}_2$ thin films.⁵² Here, it was claimed that observed magnetic anisotropy originates due to magneto crystalline anisotropy in the system, which originates due to tetragonal distortion of *bcc* Fe lattice as N atoms occupy interstitial positions. Magneto crystalline anisotropy constant (K_u) can be calculated using: $K_u = H_k \times M_s/2$,⁵² where M_s is saturation magnetization and H_k is anisotropy field which has a value close to H_s saturation field as indicated in the fig 2(a). We obtain $K_u = 5.4 \times 10^5 \text{ Jm}^{-3}$, which is close to the reported value.⁵² Additionally, obtained values of coercivity (H_C) = 10 kA/m and saturation magnetization ($4\pi M_S$) = 1.6 T. Apart from this, the ratio of remanence magnetization and M_S was found to be 0.4, indicating PMA. For the Fe-Al-N and Fe-Zr-N samples, M-H loops are square shaped with a very small value of H_C ($\sim 1 \text{ A/m}$), indicating formation of a soft magnetic phase. For Fe-Al-N and Fe-Zr-N samples the value of $4\pi M_S$ is 1.46 T and 1.39 T, respectively, which are smaller than Fe-N, due to doping of non-magnetic elements. Further, in the doped samples, an open region near the saturation field can be seen (as shown in the inset of the fig. 2(b,c)) indicating presence of some hard magnetic phase. Existence of hard magnetic phase in the samples was later confirmed by Mössbauer spectroscopy measurements which are presented in section III C.

Apart from M-H measurements we have also performed PNR measurements on these samples. It is known that for magnetic thin films, PNR is a unique technique to measure the magnetic moment very precisely irrespective of sample dimension. The difference between the critical edges of spin-up (fig. 3) and spin-down (not shown) reflectivities provide information about magnetic moment as samples were magnetically saturated.⁵⁴ Here observed Bragg peak is due to bilayer periodicity of $^{57}\text{Fe}/^{nat}\text{Fe}$ having different neutron scattering length contrast. To obtain information about the bilayer thickness and magnetic moment in the samples the data are fitted using SimulRefic software.⁵⁵ For Fe-N, Fe-Al-N and Fe-Zr-N samples bilayer thickness are 13.06 nm, 13.1 nm, and 12.3 nm, and value of the magnetic moment is $1.8 \mu_B$, $1.7 \mu_B$, and $1.65 \mu_B$, respectively. These values of magnetic moment are in agreement with those obtained from S-VSM measurements.

C. Conversion electron Mössbauer spectroscopy

Mössbauer spectroscopy is a versatile technique to probe the local structure around a resonant nuclei. From our XRD results, discussed in the section III A, it was

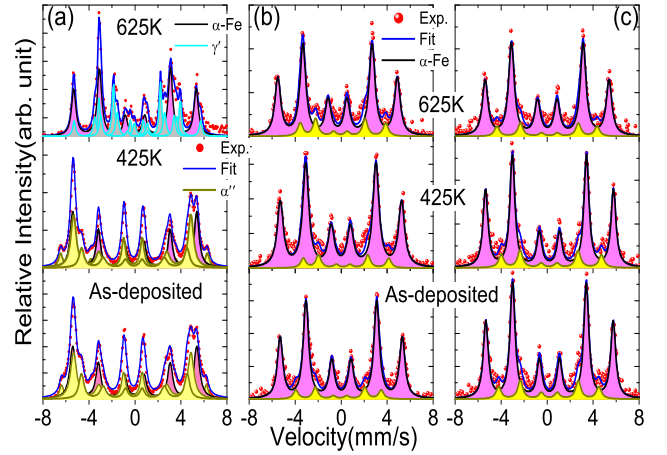


FIG. 4. (color online) CEMS spectra of Fe-N(a), Fe-Al-N(b), and Fe-Zr-N(c) thin films in the as-deposited state and after annealing at various temperatures.

observed that in the as-deposited state Fe-N films have mixed $\alpha''\text{-Fe}_{16}\text{N}_2$ and $\alpha\text{-Fe(N)}$ phases. Whereas in Al or Zr doped samples, only $\alpha\text{-Fe(N)}$ phase can be seen. Using Mössbauer spectroscopy relative volume fraction of the different Fe-N phases can be obtained. Fig. 4(a-c) shows selective CEMS spectra of Fe-N(a) Fe-Al-N(b) and Fe-Zr-N(c) thin films in the as-deposited state and after annealing at 425 K and 625 K. We fitted the observed CEMS spectra using NORMOS SITE and DIST programs.⁵⁶

CEMS spectrum of the as-deposited Fe-N sample can only be fitted assuming four sextet. Three of them corresponding to $\alpha''\text{-Fe}_{16}\text{N}_2$ phase (hyperfine field = 39 T, 31.6 T, and 28.5 T) and remaining to $\alpha\text{-Fe}$ (hyperfine field=33 T), the obtained fitting parameters correlates well with previously reported values.⁵⁷ Additionally, area of the fitted sextets can be used to calculate the relative concentration of these phases, which are tabulated in the table II. As can be seen, after annealing at 425 K the values are almost similar to as-deposited sample, but at a higher annealing temperature of 500 K (not shown) and 625 K, $\alpha''\text{-Fe}_{16}\text{N}_2$ phase disappears and γ' phase starts to grow. Observed CEMS results for the Fe-N sample correlate well with our XRD results. Moreover, from the relative area under γ' and $\alpha\text{-Fe}$ phase above 500 K, N concentration can be estimated¹⁶ which comes out to be $(11 \pm 2)\text{at.}\%$ which is in agreement with our SIMS measurements.

In comparison to Fe-N, CEMS spectra of doped samples are completely different and remains almost similar to the as-deposited samples even after annealing at 625 K, as expected from XRD results. Besides, it was found that CEMS spectra of Fe-Al-N and Fe-Zr-N samples can only be fitted assuming two components - one corresponding to $\alpha\text{-Fe}$ phase with hyperfine field about 33 T and other with a reduced hyperfine field. As our magnetization measurements on doped samples show presence of a hard

TABLE II. Volume fraction of various Fe-N phases obtained from fitting CEMS spectra. Here ‘H’ stands for a hard magnetic phase.

Temperature	Fe-N	FeAlN	FeZrN
As-deposited	59% (α'' -Fe ₁₆ N ₂) + 41% (α -Fe)	89% (α -Fe) + 11% (H)	86% (α -Fe) + 14% (H)
425 K	60% (α'' -Fe ₁₆ N ₂) + 40% (α -Fe)	90% (α -Fe) + 10% (H)	86% (α -Fe) + 14% (H)
625 K	48% (γ') + 52% (α -Fe)	88% (α -Fe) + 12% (H)	88% (α -Fe) + 12% (H)

magnetic phase, the phase formed with reduced hyperfine field may be attributed to it. The values of hyperfine field for such hard phase are 23 T for Fe-Al-N and 27 T for Fe-Zr-N samples.

It may be noted that our XRD, magnetization and CEMS measurements present a comprehensive information about the structural and magnetic properties of samples in the as-deposited state and after annealing at different temperatures. While un-doped sample undergoes phase formation upon annealing, both local and long range stability seems to get significantly improved with Al and Zr doping. However, thermal stability seems to be better with Al than with Zr. In order to understand the mechanism leading to thermal stability, we performed self-diffusion measurements of Fe and N in our samples, which will be discussed in the next section.

D. Self-diffusion measurements

In this section we present self-diffusion measurements performed using PNR, SIMS and NRR. It is known that these techniques are the only methods to probe self-diffusion in stable isotopes. While reflectivity techniques (PNR and NRR) offer an excellent depth resolution of about 0.1 nm,^{24,58–60} the information obtained from these techniques is ‘indirect’ as they are based on x-ray/neutron scattering. SIMS on the other hand provides depth profile of isotopes giving a ‘direct’ information of diffusivity. Although depth resolution of SIMS is about 5 nm, a comparison of reflectivity and SIMS provides reliable information about self-diffusion. In this work we measured Fe self-diffusion using PNR and NRR and N self-diffusion using PNR and SIMS. Complementarities of different techniques was used to get precise information of Fe and N self-diffusion.

Fig. 5 shows PNR patterns of Fe-N(a1,a2), Fe-Al-N(b1,b2), Fe-Zr-N(c1,c2) and Fe-Ti-N(d1,d2) samples in the as-deposited state and after annealing at various temperatures. In fig.(a1-d1) and fig.(a2-d2) a Bragg peak originating due to scattering length (b_n) contrast of $^{57}\text{Fe}/^{nat}\text{Fe}$ and $^{15}\text{N}/^{nat}\text{N}$, respectively. X-ray reflectivity measurements (not shown) performed on these samples do not show any Bragg peak due to lack of contrast between isotopes. It confirmed that films are chemically homogeneous. Since our samples are iron rich and a large difference between the value of b_n for ^{nat}Fe (=9.45 fm) and ^{57}Fe (=2.3 fm) exists, considerably intense Bragg peak can be seen even with 10 repetition of bilayers. However, for nitrogen, relatively smaller differ-

ence in b_n for ^{nat}N (=9.36 fm) and ^{15}N (=6.3 fm) and low nitrogen concentration (~ 11 at.%), makes it very difficult to measure nitrogen diffusion. Probably this is the reason that nitrogen self-diffusion has not yet been reported for magnetic Fe-X-N thin films. In order to get the appreciable intensity of Bragg peak, we increased bilayer thickness and the number of repetitions. From fitting of the PNR data⁵⁵ measured bilayer period for un-doped and Al, Zr or Ti doped samples are 18.8 nm, 18.4 nm, 17.6 nm, and 17.2 nm, respectively. From fig. 5(a2-d2) it can be seen, a Bragg peak of appreciable intensity due to $^{15}\text{N}/^{nat}\text{N}$ contrast can be clearly observed. Although its intensity is considerably low (as compared to $^{57}\text{Fe}/^{nat}\text{Fe}$), as expected.

To study self-diffusion, samples were annealed in a vacuum furnace at different temperatures for 1 hour at each temperature. For $^{57}\text{Fe}/^{nat}\text{Fe}$ samples, we find that the intensity of the peak does not change with annealing (fig.5(a1-d1)) indicating that up to a temperature of 475 K self-diffusion of iron is negligible. On the other hand, in $^{15}\text{N}/^{nat}\text{N}$ samples, noticeable nitrogen diffusion can be seen even at a temperature of 375 K, and at 425 K nitrogen gets almost completely diffused in all but Al doped samples as shown in fig. 5(a2-d2). Incidentally, we measured un-doped and Al doped samples kept at room temperature just after deposition and after about one year (355 days). Inset of fig. 5 compares PNR patterns of Fe-N(a2) and Fe-Al-N(b2) samples taken immediately after deposition and after 355 days kept at room temperature. It can be seen that N diffusion suppresses with Al doping even at room temperature. This is a clear indication that nitrogen self-diffusion gets remarkably suppressed with Al doping. In contrast to this, with Zr doping behavior of nitrogen diffusion is surprisingly unusual, as Zr doping results in somewhat faster nitrogen diffusion compared to un-doped Fe-N sample.

From the decay in the intensity of Bragg peak self-diffusivity in the samples can be calculated using the following expression:^{24,58–60}

$$\ln \left[\frac{I(t)}{I(0)} \right] = \frac{-8\pi^2 D t}{d^2} \quad (1)$$

where $I(0)$ is the intensity of the first order Bragg peak at time $t = 0$ (before annealing), d is the bilayer thickness and D is diffusivity. Obtained values of D for Fe-N and Fe-Al-N samples kept at room temperature for about one year comes out to be $2 \times 10^{-25} \text{m}^2 \text{s}^{-1}$ and $1 \times 10^{-25} \text{m}^2 \text{s}^{-1}$, respectively. Information about diffusivity can also be obtained from fitting of PNR data. Following the fitting procedure as mentioned in section III B, obtained values

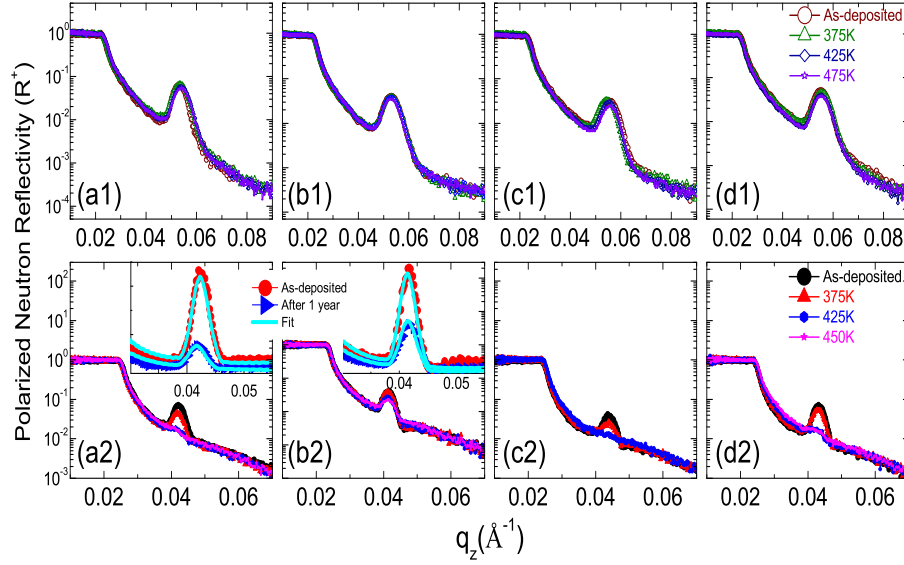


FIG. 5. (color online) PNR patterns of Sub. $[\text{Fe-X-N}]^{57}\text{Fe-X-N} \times 10$ for $X = 0$ (a1), Al (b1), Zr (c1), Ti (d1) and Sub. $[\text{Fe-X-N}]\text{Fe-X-}^{15}\text{N} \times 25$ for $X = 0$ (a2), Al (b2), Zr (c2), Ti (d2) in the as-deposited state and after annealing at various temperatures. Inset of (a2,b2) compares PNR patterns of Fe-N and Fe-Al-N samples taken just after deposition and measured after one year.

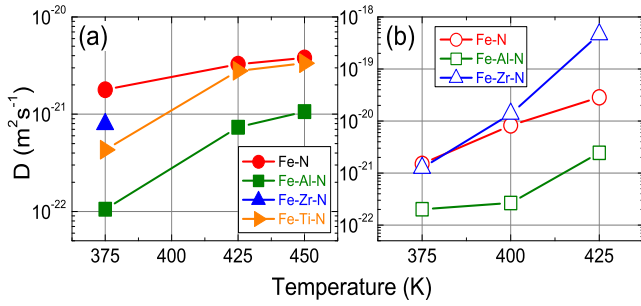


FIG. 6. (color online) Self-diffusivity of nitrogen obtained from PNR(a) and SIMS(b) measurements, solid lines are guide to eye. Typical error bars in the measurements are about the size of scatters.

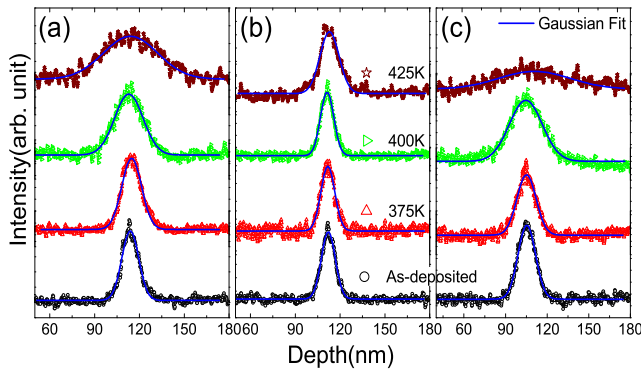


FIG. 7. (color online) ^{15}N SIMS depth profile of Sub. $[\text{Fe-X-N}(110\text{ nm})]\text{Fe-X-}^{15}\text{N}(2\text{ nm})\text{Fe-X-N}(110\text{ nm})$ trilayer samples with $X = 0$ (a), Al(b), and Zr(c) in the as-deposited state and after annealing at various temperatures.

of diffusion length are 3.5 nm and 2.5 nm for Fe-N and Fe-Al-N samples, respectively which are in close agreement with values obtained using eq. 1. It shows that using PNR we can measure diffusivity precisely down to $1 \times 10^{-25} \text{ m}^2 \text{ s}^{-1}$. Such small values of diffusivity are probably the lowest values ever measured.^{61,62}

Measured diffusivity at higher annealing temperature gives a snapshot picture for a fixed annealing time, obtained variation of D with temperature is shown in Fig 6(a). As mentioned before, we also measured nitrogen diffusion using SIMS and for this purpose we prepared a special trilayer structure $\text{Si}(\text{Sub.})[\text{Fe-X-}^{nat}\text{N}(110\text{ nm})|\text{Fe-X-}^{15}\text{N}(2\text{ nm})|\text{Fe-X-}^{nat}\text{N}(110\text{ nm})]$, Such structure is expected to give a peak when looking at ^{15}N depth profile. As samples are annealed broadening of this peak provides information about nitrogen self-diffusion. Applying thin films solution to Fick's law, the tracer concentration of ^{15}N with penetration depth(say x) can be expressed as:⁶³

$$c(x, t) = \frac{\text{const.}}{2\sqrt{\pi Dt}} \exp\left(\frac{-x^2}{4Dt}\right) \quad (2)$$

Here t is annealing time and D is the diffusion coefficient. Fig 7 shows SIMS depth profile of Fe-N, Fe-Al-N and Fe-Zr-N samples annealed at various temperatures. Here again we find that as annealing temperature is increased, broadening of ^{15}N peak is more for Fe-N and Fe-Zr-N samples as compared to Fe-Al-N sample. Fitting SIMS profile with a Gaussian function according to equation 2, yields D as:

$$D = \frac{\sigma_t^2 - \sigma_0^2}{2t} \quad (3)$$

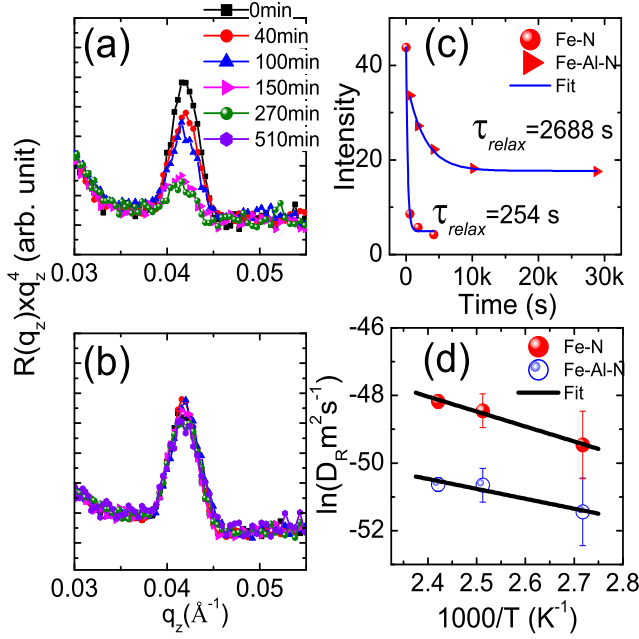


FIG. 8. (color online) PNR patterns of Sub.[Fe-N(9.4 nm)]Fe- ^{15}N (9.4 nm) $\times 25$ (a) and Sub.[Fe-Al-N(9.2 nm)]Fe-Al- ^{15}N (9.2 nm) $\times 25$ (b) samples annealed at 368 K for different time period. Variation of Bragg peak intensity with the annealing time for the above samples annealed at 415 K (c). Arrhenius behavior of nitrogen diffusion for the Fe-N and Fe-Al-N samples (d).

Here σ is the standard deviation of the Gaussian depth profile before annealing ($t=0$) and after an annealing time of t . Obtained values of D are plotted in fig. 6(b). It may be noted that the depth resolution of SIMS is relatively poor (as compared to reflectivity). Therefore, absolute values of diffusivity may differ slightly, still the behavior of nitrogen diffusion is similar to that obtained with PNR measurements. Since in Zr doped sample nitrogen diffusion was so fast that it was not possible to measure it with PNR, in SIMS measurements it can be clearly seen that with Zr doping nitrogen diffusion become even faster as compared to the un-doped sample. This is an important result, for deciding effective dopant in Fe-X-N thin films.

On the basis of above results, it can be clearly seen that nitrogen self-diffusion gets reduced only with Al doping. We therefore also performed PNR measurements with isothermal annealing experiment in Fe-N and Fe-Al-N samples at 368 K, 398 K and 413 K for different annealing time. Fig. 8(a) and (b) shows PNR patterns of Fe-N and Fe-Al-N samples annealed at 368 K for different times. Here intensity was multiplied by q_z^4 to remove decay due to Fresnel reflectivity. On comparing the reflectivity patterns, it can be clearly seen that in un-doped sample significant N diffusion started even at 368 K which increases further with increasing annealing time and attains a state of relaxation, whereas in Al doped sample only marginal diffusion takes place. Fig. 8(c) compares

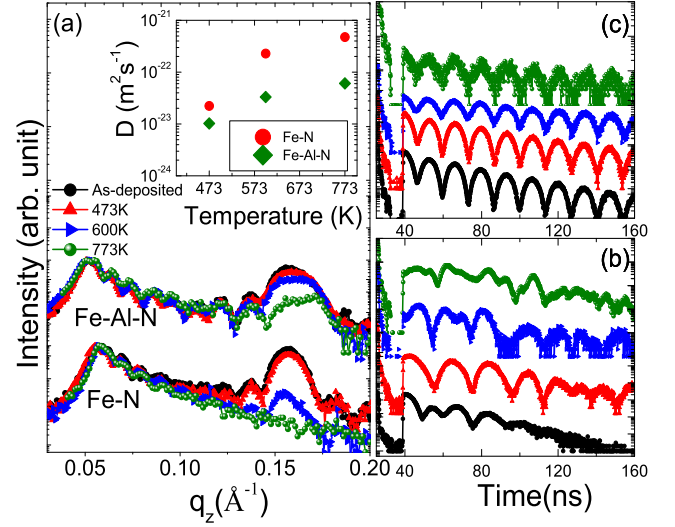


FIG. 9. (color online) NRR patterns of Sub.[Fe-N(2.2 nm)] ^{57}Fe -N(2.2 nm) $\times 10$ and Sub.[Fe-Al-N(2 nm)] ^{57}Fe -Al- ^{15}N (2 nm) $\times 10$ samples in the as-deposited state and after annealing at various temperatures (a), inset of figure shows obtained values of self-diffusivity. Corresponding NFS patterns of Fe-N (b) and Fe-Al-N (c) samples.

variation of intensity at Bragg peak with time for the Fe-N and Fe-Al-N samples annealed at 413 K. It can be seen that intensity decays exponentially with annealing time. After fitting the data using: $I(t) = I(0)\exp(-t/\tau)$, it was observed that relaxation time (τ_{relax}) for nitrogen diffusion increases by more than an order of magnitude with Al doping. Such increase in τ_{relax} provides further insight about involved diffusion mechanism, which is discussed in section IV.

It is well known that, in the relaxed state, diffusivities follows Arrhenius-type behavior given by:⁶⁴ $D_R = D_0\exp(-E/k_B T)$, with D_R is diffusivity in relaxed state and D_0 is the pre-exponential factor, E is activation energy, T is annealing temperature and k_B is Boltzman constant. Fig. 8(d) shows Arrhenius type behavior of N self-diffusion in Fe-N and Fe-Al-N thin films. A straight line fit to the data gives value of $\ln(D_0)$ and E . For Fe-N and Fe-Al-N samples values of ($\ln(D_0)$ and E) are $(-37.39 \pm 1, 0.4 \text{ eV} \pm 0.05)$ and $(-43.42 \pm 1, 0.25 \text{ eV} \pm 0.02)$, respectively. It can be seen that both $\ln(D_0)$ and E decrease with Al doping.

Comparing the value of N diffusivity (e.g. for un-doped sample) with those reported in literature (for bulk iron nitride), we find that our values are at least 3-4 orders of magnitude smaller.⁶⁵ As mentioned already, our samples are at saturation N concentration, ($\sim 11\text{at.}\%$), therefore it is expected that a large fraction of interstitial sites are filled with N atoms. Therefore, the probability of obtaining neighboring vacant interstitial sites will get reduced.⁶³

In order to get a complete picture about diffusion in our samples, it was required that iron self-diffusion should also be measured. From our neutron reflectiv-

ity measurements, we find that there is no appreciable diffusion up to a temperature of 475 K. In order to get a snapshot of diffusion, it was required that bilayer thickness (13 nm) should be decreased significantly. We therefore deposited substrate [$^{nat}\text{Fe-X-N}/^{57}\text{Fe-X-N}$] $\times 10$ (X = 0, Al) samples with bilayer thickness of about 4 nm under identical deposition conditions. In such samples Bragg peak in neutron reflectivity pattern would occur at $q_z = 0.16 \text{ \AA}^{-1}$, which is too high to be measured with neutrons due to limited flux. It is known that for ^{57}Fe , nuclear resonance reflectivity (NRR) is a very powerful technique to get precise information about the self-diffusion.⁶⁰ In addition when measured in time domain, nuclear forward scattering (NFS) is Fourier transform of energy domain reflectivity, that provides direct information about the local magnetic structure of Fe.^{66,67}

NRR measurements were performed at P01 beamline of PETRA III both in time integral and time differential modes. For ^{57}Fe the lifetime of the excited state of nucleus is about 140 ns, therefore 40 bunch mode of PETRA III was used (pulse duration of about 176 ns). In time integral mode, both electronic (prompt with few ns) and nuclear (delayed 40-140 ns) reflectivities can be measured simultaneously as they occur in different time windows and their scattering amplitude is given by : $F = F_{\text{electronic}} + F_{\text{nuclear}}$.^{60,67}

NRR measurements in time integral mode were carried out in θ - 2θ mode and are shown in fig. 9(a). On the other hand, NFS measurements were performed by sitting at the Bragg peak position and delayed photons were measured in time differential mode from 40 ns to 150 ns (within a bunch). The NFS spectra show quantum beat pattern spread-over delayed time, which arises due to interference between various hyperfine field acting at the resonant nuclei.⁶⁶

Following a similar approach as mentioned for neutron reflectivity measurements, Fe self-diffusion was measured by annealing the samples at different temperatures and performing NRR measurements subsequently. Fig. 9(a) shows NRR patterns of Fe-N and Fe-Al-N samples in the as-deposited state and after annealing samples at different temperatures. It can be seen that up to a temperature of 473 K, Fe diffusion is negligible (also seen from PNR measurements fig. 5) in both samples. In un-doped sample Fe diffusion is appreciable at 600 K while at 773 K it diffuses completely. Whereas in Al doped sample, only a marginal diffusion can be seen at 600 K while at 773 K Bragg peak can still be seen. The inset of fig. 9(a) compares Fe diffusivity obtained from the decay in intensities of the Bragg peak using the equation 1. As expected, Fe diffusivity suppress significantly with Al doping. In a recent study Fe self-diffusion was measured in ion beam sputtered Fe-N samples prepared using Al and Zr doping and found Fe diffusion suppresses both with Al and Zr doping.⁶⁸

Corresponding NFS pattern obtained at the Bragg peak position are given in fig. 9(b) and (c) for Fe-N and Fe-Al-N samples, respectively. It can be seen that for

Fe-N sample somewhat complex NFS pattern arises due to interference between different hyperfine field present in the sample. Whereas in case of Fe-Al-N sample due to the predominant presence of single hyperfine field NFS spectra shows uniform quantum beats decaying with time. Moreover, NFS spectra for Fe-N sample shows variation with annealing indicating different phase formation, which are correlated with our XRD and CEMS results discussed in section III A and III C. In case of Al doped sample no appreciable change in the NFS pattern can be observed, it suggests that the local magnetic structure also gets stabilized with Al doping. These results are consistent with our XRD and CEMS measurements.

IV. DISCUSSION

Combining results discussed above, a picture about the diffusion mechanism and the influence of dopants on diffusion can be drawn. We observed that Fe and N self-diffusion takes place in different temperature regimes. Up to a temperature of about 450 K, N diffusion dominates and Fe diffusion is negligible, only above 450 K considerable Fe diffusion can be observed. Importantly, both the structure and the magnetic properties remain almost unchanged even when nitrogen diffuses completely. It indicates that N diffusion has no significant role in the structural or magnetic changes in our samples. On the other hand, variation in the structural and magnetic properties seems to be driven by Fe self-diffusion which starts above 450 K. However, dopants have clear intervention in affecting self-diffusion of both Fe and N.

First, we will discuss the role of dopants on influencing N self-diffusion. It is known that up to a concentration of $\sim 11\text{at.}\%$, N atoms occupies interstitial sites within the Fe lattice. Numerous studies on self-diffusion behavior of light elements such as H, C, O, N etc. reveal that they follow interstitial-type diffusion mechanism.⁶⁹⁻⁷² In the course of interstitial diffusion, N atoms try to find most equilibrium interstitial site by crossing a saddle point barrier. Moreover, interstitial diffusion is strongly affected by pressure which alters available interstitial volume for diffusing N atoms.⁷³ In case of un-doped sample, due to the absence of any impeding force, N diffusion leads to its redistribution within the lattice. This redistribution favors nitrogen ordering, as observed from the sharpening in the peak corresponding to α'' phase in our XRD results (fig 1). As mentioned in III A, with Al doping lattice volume decreases by $\sim 0.5\%$. This will also decrease the available interstitial volume for the diffusing N atoms. Therefore the probability for finding equilibrium interstitial sites may get reduced, which may result in slower N diffusion or a larger relaxation time, as observed with Al doping. On the contrary, lattice volume with Zr doping increases by $\sim 2\%$. In this situation creation of extra equilibrium interstitial sites may occur, accelerating the diffusion process of N atoms. Similarly, enhanced diffusion with Ti doping can be understood.

As pointed out earlier, thermal stability of Fe-X-N thin films are significantly affected by self-diffusion of Fe. Our results show that doping of Al has notably reduced the self-diffusion of Fe. Although, we find that the structure and the magnetic stability gets improved with both Al as well as Zr doping. It indicates that the atomic size of dopants does not matter in suppressing Fe self-diffusion. It seems that the role of dopants on influencing the self-diffusion of Fe is completely different from N diffusion. Since ΔH for nitride formation of dopants is low, there is a large probability that X-N layer may be formed in the grain boundary region, as observed in some reports.^{47,74} This X-N layer may act as a diffusion barrier for Fe.⁷⁵ Moreover, this barrier layer seems to have multiple effects as it not only suppresses Fe self-diffusion, it also hinders grain growth, leading to improved soft magnetic properties as observed in our samples with Al or Zr doping. The improvement in soft-magnetic properties of Fe-N thin films with dopants was also found in previous reports.^{44,46,51} Somewhat superior thermal stability with Al doping can also be understood from the fact that only with Al doping N diffusion suppresses.

V. CONCLUSION

In the present work we have studied the role of Fe and N self-diffusion on influencing the structure, magnetic properties and thermal stability of Fe-X-N thin films. It was observed that with Al or Zr doping thermal stability gets significantly improved. Additionally, magnetization measurements revealed that soft-magnetic properties also gets improved with dopants. To understand the observed effects, detailed Fe and N self-diffusion measure-

ments were performed. It was found that dopants have clear intervention in affecting Fe and N self-diffusion, however, the mechanism leading to the suppression of Fe and N self-diffusion is different. In case of N self-diffusion, atomic size of dopants plays a crucial role. It was observed that N diffusion gets significantly reduced when the atomic size of dopants is smaller than that of Fe. A dopant with smaller size lead to compression in the Fe lattice whereas lattice expansion takes place when a larger (than Fe) dopant is used. Such lattice distortion caused by dopants results in alteration of available interstitial volume for diffusing N atoms. On the other hand Fe self-diffusion gets suppressed with any dopants, if their heat of formation is significantly smaller than that of Fe-N. This happens due to the formation of a diffusion barrier layer which not only suppresses self-diffusion of Fe but also hinders the grain growth leading to improved soft-magnetic properties. In addition it can be concluded that N diffusion has less significant role (as compared to Fe) in affecting the thermal instability in Fe-N thin films.

ACKNOWLEDGMENTS

A part of this work was performed at AMOR, Swiss Spallation Neutron Source, Paul Scherrer Institute, Villigen, Switzerland and at P01 beamline, PETRA III, DESY, Germany. We acknowledge Department of Science and Technology, New Delhi for providing financial support to carry out PNR and NRR experiments. We acknowledge V. R. Reddy for CEMS, R. J. Chaudhary for S-VSM and Layanta Behera for help provided in XRD and SIMS measurements. One of the authors (AT) thanks to CSIR India for research fellowship.

-
- * mgupta@csr.res.in/dr.mukul.gupta@gmail.com
- ¹ K. H. Jack Proc. R. Soc. Lond. Ser. A Math. and Phys. Sci. **208**, 200 (1951).
 - ² C. Navío, J. Alvarez, M. J. Capitan, F. Yndurain, and R. Miranda, Phys. Rev. B **78**, 155417 (2008).
 - ³ J. M. Gallego, S. Y. Grachev, D. M. Borsa, D. O. Boerma, D. Écija, and R. Miranda, Phys. Rev. B **70**, 115417 (2004).
 - ⁴ S. Kokado, N. Fujima, K. Harigaya, H. Shimizu, and A. Sakuma, Phys. Rev. B **73**, 172410 (2006).
 - ⁵ T. Liapina, A. Leineweber, and E. Mittemeijer, Scripta Mater. **48**, 1643 (2003).
 - ⁶ X. zhao Ding, F. min Zhang, J. sheng Yan, H. lie Shen, X. Wang, X. huai Liu, and D.-F. Shen, J. Appl. Phys. **82**, 5154 (1997).
 - ⁷ M. H. Kryder, IEEE Trans. Magn. **25**, 4358 (1989).
 - ⁸ M. Georgieva, N. Telling, P. Grundy, C. Faunce, and G. Jones, J. Appl. Phys. **96**, 2923 (2004).
 - ⁹ H. Jiang, K. Tao, and H. Li, J. Phys.: Condens. Matter **6**, L279 (1994).
 - ¹⁰ H. Sawada, A. Nogami, T. Matsumiya, and T. Oguchi, Phys. Rev. B **50**, 10004 (1994).
 - ¹¹ N. Kardonina, A. Yurovskikh, and A. Kolpakov, Met. Sci. Heat Treat. **52**, 457 (2011).
 - ¹² P. Schaaf, Prog. Mater. Sci. **47**, 1 (2002).
 - ¹³ D. M. Borsa and D. O. Boerma, Hyperfine Interact. **151-152**, 31 (2003).
 - ¹⁴ R. Gupta and M. Gupta, Phys. Rev. B **72**, 024202 (2005).
 - ¹⁵ J. Das, S. S. Kalarickal, K.-S. Kim, and C. E. Patton, Phys. Rev. B **75**, 094435 (2007).
 - ¹⁶ R. Gupta, A. Gupta, W. Leitenberger, and R. Rüffer, Phys. Rev. B **85**, 075401 (2012).
 - ¹⁷ A. Gupta, R. Dubey, W. Leitenberger, and U. Pietsch, Appl. Phys. Lett. **92**, 052504 (2008).
 - ¹⁸ T. K. Kim and M. Takahashi, Appl. Phys. Lett. **20**, 492 (1972).
 - ¹⁹ C. Navío, J. Alvarez, M. J. Capitan, J. Camarero, and R. Miranda, Appl. Phys. Lett. **94**, 263112 (2009).
 - ²⁰ D. C. Sun, C. Lin, and E. Y. Jiang, J. Phys.: Condens. Matter **7**, 3667 (1995).
 - ²¹ M. Gupta, A. Gupta, S. Rajagopalan, and A. K. Tyagi, Phys. Rev. B **65**, 214204 (2002).
 - ²² S. Chakravarty, M. Gupta, A. Gupta, S. Rajagopalan, A. Balamurugan, A. Tyagi, U. Deshpande, M. Horisberger,

- and T. Gutberlet, *Acta Mater.* **57**, 1263 (2009).
- ²³ Y. Ding and C. A. Jr., *IEEE Trans. Magn.* **42**, 5 (2006).
 - ²⁴ M. Gupta, A. Tayal, A. Gupta, R. Gupta, J. Stahn, M. Horisberger, and A. Wildes, *J. Appl. Phys.* **110**, 123518 (2011).
 - ²⁵ N. G. Chechenin, A. van Veen, H. Schut, A. R. Chezan, D. O. Boerma, T. Vystavel, and J. T. M. D. Hosson, *J. Phys.: Condens. Matter* **15**, 7663 (2003).
 - ²⁶ N. Hasegawa and M. Saito, *J. Magn. Soc. Jpn.* **14**, 313 (1990).
 - ²⁷ H. Y. Wang, E. Y. Jiang, Z. W. Ma, Y. J. He, and H. S. Huang, *J. Phys.: Condens. Matter* **11**, 989 (1999).
 - ²⁸ N. Ishiwata, C. Wakabayashi, and H. Urai, *J. Appl. Phys.* **69**, 5616 (1991).
 - ²⁹ H. Ono, M. Fujinaga, T. Yonemoto, and T. Miyagawa, *J. Appl. Phys.* **73**, 2438 (1993).
 - ³⁰ Y. Takeshima, N. Ishiwata, T. Korenari, and H. Urai, *J. Appl. Phys.* **73**, 6576 (1993).
 - ³¹ G. Qiu and J. A. Barnard, *J. Appl. Phys.* **75**, 6934 (1994).
 - ³² F. Roozeboom and F. W. A. Dirne, *J. Appl. Phys.* **77**, 5293 (1995).
 - ³³ B. Viala, M. K. Minor, and J. A. Barnard, *J. Appl. Phys.* **80**, 3941 (1996).
 - ³⁴ H. Y. Wang, E. Y. Jiang, H. L. Bai, P. Wu, Y. Wang, and F. F. Gong, *J. Phys.: Condens. Matter* **9**, 8443 (1997).
 - ³⁵ L. Varga, H. Jiang, T. J. Klemmer, W. D. Doyle, and E. A. Payzant, *J. Appl. Phys.* **83**, 5955 (1998).
 - ³⁶ Y. Chen, C. Qian, C.-Y. Hung, and M. Miller, *J. Appl. Phys.* **87**, 5864 (2000).
 - ³⁷ Y.-K. Liu and M. H. Kryder, *Appl. Phys. Lett.* **77**, 426 (2000).
 - ³⁸ A. Chezan, C. Craus, N. Chechenin, L. Niesen, and D. Boerma, *Phys. Status Solidi A* **189**, 833 (2002).
 - ³⁹ J. Rantschler, Y. Ding, S.-C. Byeon, and C. Alexander, *J. Appl. Phys.* **93**, 6671 (2003).
 - ⁴⁰ Y.-K. Liu, M. H. Kryder, D. H. Ryan, and Z. Altounian, *J. Appl. Phys.* **93**, 6471 (2003).
 - ⁴¹ A. Kamzin, F. Wei, Z. Yang, and S. Kamzin, *Tech. Phys. Lett.* **31**, 461 (2005).
 - ⁴² S. S. Kalarickal, P. Krivosik, J. Das, K. S. Kim, and C. E. Patton, *Phys. Rev. B* **77**, 054427 (2008).
 - ⁴³ F. Xu, S. Li, and C. K. Ong, *J. Appl. Phys.* **109**, 07D322 (2011).
 - ⁴⁴ R. Gupta, A. Tayal, S. M. Amir, M. Gupta, A. Gupta, M. Horisberger, and J. Stahn, *J. Appl. Phys.* **111**, 103520 (2012).
 - ⁴⁵ M. Kopcewicz, J. Jagielski, G. Gawlik, and A. Grabias, *J. Appl. Phys.* **78**, 1312 (1995).
 - ⁴⁶ N. Ishiwata, C. Wakabayashi, and H. Urai, *J. Appl. Phys.* **69** (1991).
 - ⁴⁷ H. Y. Wang, E. Y. Jiang, H. L. Bai, P. Wu, Y. Wang, and F. F. Gong, *J. Physics: Condensed Matter* **9**, 8443 (1997).
 - ⁴⁸ F. Tessier, A. Navrotsky, R. Niewa, A. Leineweber, H. Jacobs, S. Kikkawa, M. Takahashi, F. Kanamaru, and F. J. DiSalvo, *Solid State Sci.* **2**, 457 (2000).
 - ⁴⁹ D. B. Evans, *Determination of Nitride Solubility In The Solvent Liquid Iron* (Ph.D. Thesis, University of Michigan, 1963).
 - ⁵⁰ E. Clementi, D. L. Raimondi, and W. P. Reinhardt, *J. Chem. Phys.* **47**, 1300 (1967).
 - ⁵¹ A. Tayal, M. Gupta, A. Gupta, M. Horisberger, and J. Stahn, *Thin Solid Films* **536**, 39 (2013).
 - ⁵² N. Ji, M. S. Osofsky, V. Lauter, L. F. Allard, X. Li, K. L. Jensen, H. Ambaye, E. Lara-Curzio, and J.-P. Wang, *Phys. Rev. B* **84**, 245310 (2011).
 - ⁵³ B. D. Cullity, *Elements of X-ray Diffraction* (Addison-Wesley, MA, 1978).
 - ⁵⁴ S. J. Blundell and J. A. C. Bland, *Phys. Rev. B* **46**, 3391 (1992).
 - ⁵⁵ F. Ott, *SimulReflec V1.7* (2011).
 - ⁵⁶ R. Brand, NORMOS, Wissenschaftlich Elektronik GmbH, Starnberg (1995).
 - ⁵⁷ M. Takahashi and H. Shoji, *J. Magn. Magn. Mater.* **208**, 145 (2000).
 - ⁵⁸ M. P. Rosenblum, F. Spaepen, and D. Turnbull, *Appl. Phys. Lett.* **37**, 184 (1980).
 - ⁵⁹ J. Speakman, P. Rose, J. Hunt, N. Cowlam, R. E. Somekh, and A. Greer, *J. Magn. Magn. Mat.* **156**, 411 (1996).
 - ⁶⁰ A. Gupta, M. Gupta, S. Chakravarty, R. Rüffer, H.-C. Wille, and O. Leupold, *Phys. Rev. B* **72**, 014207 (2005).
 - ⁶¹ H. Schmidt, M. Gupta, and M. Bruns, *Phys. Rev. Lett.* **96**, 055901 (2006).
 - ⁶² H. Schmidt, M. Gupta, T. Gutberlet, J. Stahn, and M. Bruns, *Acta Mater.* **56**, 464 (2008).
 - ⁶³ H. Mehrer, *Diffusion in solids: fundamentals, methods, materials, diffusion-controlled processes*, Vol. 155 (Springer, 2007).
 - ⁶⁴ F. Faupel, W. Frank, M. P. Macht, H. Mehrer, K. Rätzke, H. Schober, S. K. Sharma, and H. Teichler, *Rev. Mod. Phys.* **75**, 237 (2003).
 - ⁶⁵ J. da Silva and R. B. McLellan, *Materials Science and Engineering* **26**, 83 (1976).
 - ⁶⁶ E. Gerda, R. Rüffer, R. Hollatz, and J. P. Hannon, *Phys. Rev. Lett.* **57**, 1141 (1986).
 - ⁶⁷ R. Röhlberger, J. Bansmann, V. Senz, K. L. Jonas, A. Bettac, K. H. Meiwes-Broer, and O. Leupold, *Phys. Rev. B* **67**, 245412 (2003).
 - ⁶⁸ A. Tayal, M. Gupta, D. Kumar, V. R. Reddy, A. Gupta, S. M. Amir, P. Korelis, and J. Stahn, *J. Appl. Phys. (Communicated)*.
 - ⁶⁹ J. Snoek, *Physica* **8**, 711 (1941).
 - ⁷⁰ C. P. Flynn and A. M. Stoneham, *Phys. Rev. B* **1**, 3966 (1970).
 - ⁷¹ C. Zener, *J. Appl. Phys.* **22** (1951).
 - ⁷² C. A. Wert, *J. Appl. Phys.* **21** (1950).
 - ⁷³ A. Bosman, P. Brommer, and G. Rathenau, *Physica* **23**, 1001 (1957).
 - ⁷⁴ Y. Ding, S. C. Byeon, and J. Alexander, *C., IEEE Trans. Magn.* **37**, 1776 (2001).
 - ⁷⁵ M.-A. Nicolet, *Thin Solid Films* **52**, 415 (1978).